Structure−Function in *Escherichia coli* Iron Superoxide Dismutase: Comparisons with the Manganese Enzyme from *Thermus thermophilus*[†,‡]

Myoung S. Lah,[§] Melinda M. Dixon, Katherine A. Pattridge, William C. Stallings,[∥] James A. Fee,[⊥] and Martha L. Ludwig*

Biophysics Research Division and Department of Biological Chemistry, University of Michigan, Ann Arbor, Michigan 48109

Received July 7, 1994[⊗]

ABSTRACT: The crystal structure of dimeric Fe(III) superoxide dismutase (SOD) from *Escherichia coli* (3006 protein atoms, 2 irons, and 281 solvents) has been refined to an R of 0.184 using all observed data between 40.0 and 1.85 Å (34 879 reflections). Features of this structure are compared with the refined structure of MnSOD from *Thermus thermophilus*. The coordination geometry at the Fe site is distorted trigonal bipyramidal, with axial ligands His26 and solvent (proposed to be OH^-), and in-plane ligands His73, Asp156, and His160. Reduction of crystals to the Fe(II) state does not result in significant changes in metal−ligand geometry (R = 0.188 for data between 40.0 and 1.80 Å). The arrangement of iron ligands in Fe(II) and Fe(III)SOD closely matches the Mn coordination found in MnSOD from *T. thermophilus* [Ludwig, M. L., Metzger, A. L., Pattridge, K. A., & Stallings, W. C. (1991) *J. Mol. Biol. 219*, 335−358]. Structures of the Fe(III) azide (40.0−1.8 Å, R = 0.186) and Mn(III) azide (20.0−1.8 Å, R = 0.179) complexes, reported here, reveal azide bound as a sixth ligand with distorted octahedral geometry at the metal; the in-plane ligand−Fe−ligand and ligand−Mn−ligand angles change by 20−30° to coordinate azide as a sixth ligand. However, the positions of the distal azide nitrogens are different in the FeSOD and MnSOD complexes. The geometries of the Fe(III), Fe(II), and Fe(III)−azide species suggest a reaction mechanism for superoxide dismutation in which the metal alternates between five- and six-coordination. A reaction scheme in which the ligated solvent acts as a proton acceptor in the first half-reaction [formation of Fe(II) and oxygen] is consistent with the pH dependence of the kinetic parameters and spectroscopic properties of Fe superoxide dismutase.

Superoxide dismutases (SODs) are divided into two structural families. The Cu/Zn SODs, which were the first superoxide dismutases to be characterized (Fridovich, 1974) and the first to be analyzed by X-ray methods (Tainer et al., 1982), are homodimers whose fundamental structural motif is a β-barrel. In the Cu/Zn enzymes, the metals are bound by sequences connecting the barrel strands and are on opposite sides of the dimer with the Cu atoms separated by 33.8 Å. The second family of SODs, prevalent in bacteria and in mitochondria (Bannister et al., 1987), utilizes either Fe or Mn to catalyze dismutation of O_2^- and constitutes a close-knit group of proteins in which sequences (Chan et al., 1990; Schinina et al., 1987) are highly conserved and structures are very similar. Mn- and FeSODs occur as homodimers and occasionally as homotetramers. The monomers fold into two helix-rich domains with Mn or Fe bound by two residues from each domain. Dimer contacts occur at an interface bridging two metal sites that are separated by about 18 Å, and the path by which substrate presumably reaches the metal is lined by residues from both monomers (Stallings et al., 1983, 1985, 1992; Ringe et al., 1983; Ludwig et al., 1991).

The initial structures of the Fe-containing dismutases from *Escherichia coli* and from *Pseudomonas ovalis* were based on data at resolutions of 3.1 and 2.9 Å, respectively (Stallings et al., 1983; Ringe et al., 1983). The structure analysis of FeSOD from *P. ovalis* was subsequently extended to a resolution of 2.1 Å (Stoddard et al., 1990a). In this paper we describe structures of *E. coli* FeSOD at resolutions of 1.8−1.85 Å and compare features of the protein fold and the metal-binding site of this FeSOD with *Thermus thermophilus* MnSOD, which has been refined at a resolution of 1.8 Å (Ludwig et al., 1991). Crystal structures have also been determined for the Mn-containing SODs from *Bacillus stearothermophilus* (Parker & Blake, 1988) and for recombinant enzymes corresponding to human mitochondrial MnSOD (Borgstahl et al., 1992; Wagner et al., 1993).

It is generally accepted that in all SODs the metal ion catalyzes dismutation of superoxide through a cyclic oxidation−reduction mechanism as shown below (ignoring protonation), with both reduction and reoxidation presumed to occur in inner sphere complexes:

$$M^{3+} + O_2^- \rightarrow M^{2+} + O_2$$

$$M^{2+} + O_2^- \rightarrow M^{3+} + H_2O_2$$

This type of mechanism has been widely discussed (Lavelle et al., 1977; Tainer et al., 1983; Getzoff et al., 1989),

[†] Supported by NIH Grant GM16429.

[‡] The Protein Data Bank access codes for the coordinate sets are Fe(III)SOD, 1ISB; Fe(II)SOD, 1ISA; Fe(III)SOD-azide, 1ISC; Mn(III)SOD-azide, 1MNG.

* Author to whom correspondence should be addressed. Telephone: (313) 747-2736. Fax: (313) 764-3323. E-mail: ludwig@norway.biop.umich.edu.

[§] Present address: Chemistry Department, Hanyang University, 396 Taehakdong Ansan, Kyunggido, Korea.

[∥] Present address: Monsanto-Searle, 700 Chesterfield Village, St. Louis, MO 63198.

[⊥] Present address: Department of Biology, University of California San Diego, La Jolla, CA 92093.

[⊗] Abstract published in *Advance ACS Abstracts,* January 15, 1995.

0006-2960/95/0434-1646$09.00/0

Table 1: Summary of Data Sets

	Fe(III)SOD	Fe(II)SOD	azide−Fe(III)SOD	azide−Mn(III)SOD
crystal size (mm)	0.6 × 0.4 × 0.3	0.6 × 0.4 × 0.3	0.7 × 0.5 × 0.4	0.5 × 0.4 × 0.3
space group	$P2_12_12_1$	$P2_12_12_1$	$P2_12_12_1$	$P4_12_12$
cell parameters (Å)	$a = 81.62$	$a = 81.55$	$a = 81.61$	$a = 146.8$
	$b = 75.28$	$b = 75.08$	$b = 75.16$	$b = 146.8$
	$c = 71.61$	$c = 71.53$	$c = 71.58$	$c = 55.6$
resolution range (Å)	40.0−1.85	40.0−1.80	40.0−1.80	20.0−1.80
reflections ($F > 0.1$)	34 879	37 923	38 384	52 673
completeness (%)	93	92	94	93
redundancy	5.9	4.2	4.9	6.5
R_{sym} (%)	8.35	5.91	5.01	7.7
average $I/\sigma(I)$	15.4	16.2	15.3	10.6

Table 2: Refinements

run	resolution	reflections[a]	atoms (inc. polar H)	solvents	stage[a]	R_{init}	R_{final}
			Fe(III)SOD				
A	5.0−2.0	23 617 (27 114)	4197	185	PB	0.173	0.165
B	40.0−2.0	25 460 (29 213)	4197	185	PB	0.188	0.182
C	40.0−2.0	25 460 (29 213)	4302	220	PB	0.181	0.175
D	5.0−2.0	25 743 (26 357)	4473	277	R	0.316	0.193
	6.0−1.85	32 805 (33 859)	4473	277	PB	0.200	0.172
E	40.0−1.85	34 879	4473	277	PB	0.187	0.187
F	40.0−1.85	34 879	4713	357	PB	0.184	0.181
					Bocc	0.181	0.182
					PB	0.181	0.177
G	40.0−1.85	34 879	4485	281	PB	0.185	0.184
			Fe(II)SOD				
A	5.0−2.0	26 372 (27 086)	3642	0	R, PB	0.305	0.215
B	5.0−2.0	26 372 (27 086)	4197	185	PB	0.204	0.186
C	40.0−2.0	28 444 (29 170)	4212	190	PB	0.199	0.192
D	40.0−2.0	28 444 (29 170)	4314	224	PB	0.190	0.184
E	40.0−1.8	37 923	4314	224	PB	0.202	0.194
F	40.0−1.8	37 923	4470	276	PB, Bocc	0.191	0.188
G	40.0−1.8	37 923	4470	276	SA, P, Bocc	0.187	0.184
H	40.0−1.8	37 923	4350	236	PB	0.188	0.188
			azide−Fe(III)SOD				
A	5.0−1.8	34 900 (36 428)	3642	0	R, PB	0.350	0.262
B	5.0−1.8	34 900 (36 428)	3654	2[b]	PB	0.237	0.218
C	40.0−1.8	36 948 (36 384)	4320	224	PB	0.215	0.196
D	40.0−1.8	36 948 (38 384)	4521	291	PB	0.205	0.185
E	40.0−1.8	36 948 (38 384)	4650	334	PB	0.186	0.182
F	40.0−1.8	36 948 (38 384)	4650	334	PB, Bocc	0.182	0.182
G	40.0−1.8	38 384	4650	334	P, Bocc, P	0.186	0.185
H	40.0−1.8	38 384	4641	331	PB	0.185	0.179
I	40.0−1.8	38 384	4767[d]	333[d]	SA, P, Bocc[d]	0.181	0.180
J	40.0−1.8	38 384	4584	272	PB	0.186	0.186
			azide−Mn(III)SOD				
A	20.0−1.8	52 673	4539	187	R	0.218	0.213
B	20.0−1.8	52 673	4533	185[c]	PB	0.214	0.192
C	20.0−1.8	52 673	4545	187[b]	P, Bocc	0.191	0.184
D	20.0−1.8	52 673	4671[d]	189[d]	SA, P, Bocc[d]	0.224	0.181
E	20.0−1.8	52 673	4710	202	PB	0.182	0.179

[a] Total number of reflections is indicated in parentheses. P, positional refinement; B, isotropic temperature factor refinement; R, rigid body refinement; Bocc, group B and occupancy refinement of solvents; SA, simulated annealing from 1000 K. The total number of reflections available is indicated in parentheses. [b] Azide ions from each chain are included at this and subsequent steps in the refinements. [c] Refined with Mn-liganded solvents removed. [d] Alternate conformation of the metal ligands (without azide) included in this and the following step (see text).

and detailed kinetic analyses of the reactions of *E. coli* FeSOD (Bull & Fee, 1985) and *T. thermophilus* MnSOD (Bull et al., 1991) have been presented. The interactions of *E. coli* FeSOD with azide, a presumed substrate mimic, have been examined by steady-state (Bull & Fee, 1985), T-jump (Fee et al., 1981), and NMR relaxation (Dooley et al., 1987) techniques. Changes in spectral signals from the metal are consistent with formation of an inner-sphere Fe(III)−azide complex. Initial interpretations (Bull & Fee, 1985) assumed that, in binding to iron, azide (or substrate) displaces a solvent ligand.

A primary goal in the present study was to determine the structures of the azide complex(es) and of the Fe(II) species at high resolution for correlation with the kinetic and spectroscopic data. Preliminary analysis of the azide complex of *E. coli* Fe(III)SOD at 2.5 Å resolution (Stallings et al., 1991) indicated that contrary to expectations azide does not displace other metal ligands but instead expands the coordination sphere of the central metal ion. We have summarized some of these earlier results in symposium reports and have proposed reaction schemes for superoxide dismutation by FeSOD, incorporating intermediates analo-

gous to the azide complex (Stallings et al., 1991, 1992). In this paper we describe the metal−ligand geometry of Fe(III)SOD, Fe(III)SOD−azide, Mn(III)SOD−azide, and Fe(II)SOD and suggest a detailed reaction scheme for FeSOD. The accompanying paper (Tierney et al., 1995) presents an analysis of EXAFS measurements on Fe(III)SOD and the Fe(III)SOD−azide complex.

MATERIALS AND METHODS

FeSOD Crystals and Data Collection. Native crystals were grown from ammonium sulfate at pH 4.5−4.7 as described (Stallings et al., 1983). The crystals are orthorhombic in space group $P2_12_12_1$, with $a = 81.62$, $b = 75.28$, and $c = 71.61$ Å and the dimeric molecule constituting the asymmetric unit. Native data for the initial model building and refinement of oxidized Fe(III)SOD at 2.0 Å had been collected at 4 °C and pH 4.8 at the UCSD Multiwire Detector Facility; for later stages of the analysis, we substituted data to 1.85 Å collected in-house from one crystal at 4 °C and pH 7.0 using a dual multiwire detector (Area Detector Systems Corporation, San Diego). Crystals were soaked overnight in holding solution (2.4 M ammonium sulfate buffered with potassium phosphate at pH 7.0) before data collection. The 215 280 observations were scaled and merged to yield 34 879 unique reflections representing 93% of the theoretical total from 40.0 to 1.85 Å (Table 1).

Crystals were reduced in a nitrogen-flushed glove box by soaking overnight in holding solution with excess dithionite buffered at pH 7.0. Reduction of the metal center could be assessed by visual observation, since the yellow color of oxidized Fe(III)SOD crystals bleaches on reduction. Data were collected from one Fe(II)SOD crystal to 1.8 Å resolution at 4 °C on the ADSC area detector. The azide complex of Fe(III)SOD was prepared by soaking overnight in holding solution with 100 mM sodium azide buffered at pH 7.0; complex formation was evident from the orange-red color of the crystals.

Mn(III)SOD Crystals and Data Collection. Crystals of the native enzyme from *T. thermophilus*, grown as described (Stallings et al., 1984), were soaked overnight in buffered 50% ammonium sulfate (pH 7.0) containing 100 mM azide. The dichroic purple MnSOD crystals should bleach slightly on addition of azide (Whittaker & Whittaker, 1991), but the changes are small and difficult to observe during soaking. Data to 1.8 Å were collected from two crystals at room temperature. A summary of the X-ray measurements is presented in Table 1.

Crystallographic Refinement: General Strategies. Except for the initial steps in refinement of Fe(III)SOD, computations were conducted with X-PLOR, using standard protocols (Brünger, 1992). Parameters for energies of bonded and nonbonded protein interactions were from the set PRO19X or HCSDX; parameters for the metal−ligand interactions are described below. Difference maps were inspected after each round of refinement and the model atoms were adjusted as necessary with the aid of the graphics program TOM (Cambillau & Horjales, 1987). Solvents were assigned to density peaks $>3\sigma$ in ($|F_o| - |F_c|$) maps if they made acceptable polar or nonpolar contacts with other atoms. After adjustment of positional parameters and individual B factors for all protein and solvent atoms, occupancies and group temperature factors of solvents, metals, and nonprotein ligands were refined. As refinement progressed, the resolution ranges and numbers of measured reflections were gradually increased; the final rounds included all observed reflections. The steps in refinement are summarized in Table 2.

The solvent models were re-examined during the last stage of refinement. Solvents with very small scattering contributions were removed from the atom lists for a final round of positional and B refinement of all atoms. As shown in Table 2, the R value increased after removing these solvents. A conservative assignment of solvents is consistent with our earlier refinements (Ludwig et al., 1991).

Restraints on Metal−Ligand Geometry during Refinement. The nominal metal−ligand bond distance for the trivalent metals was set to 1.90 Å for metal−oxygen bonds and 2.00 Å for metal−nitrogen bonds; the corresponding distances for Fe(II) and the azide complexes were 2.00 and 2.10 Å. The target parameters for angles at the metals corresponded to ideal trigonal bipyramidal geometry in Fe(III)SOD and Fe(II)SOD and to distorted octahedral geometry (see Table 4) in the azide complexes of Fe(III)SOD and Mn(III)SOD. Force constants were 65.0 kcal/mol·Å^2 for distances and 5.0 kcal/mol·rad^2 for angles, one-tenth of the values assigned for bonded backbone or side chain atoms. To assess the dependence of the results on the energy terms, we carried out a series of tests with Fe(III)SOD, starting with the coordinates from step E (Table 2). Removing restraints altogether (force constants of 0.0 for bond lengths and angles) did not alter the final positions of the ligand atoms, and difference maps were featureless at 3σ. With large force constants (650 and 50) and long ideal distances (3.0 Å), positional refinement moved the ligand atoms to distances about 2.8 Å from the Fe, and peaks in difference maps indicated that these positions were incorrect. Continued refinement with small force constants returned the atoms to positions close to those reported in Table 4. However, the metal−ligand bond lengths do show some dependence on the target values that are chosen. For example, with 2.00 Å as the nominal length for all bonds, the average iron−ligand distance for Fe(II)SOD is 2.00 Å, but, with 2.10 Å as the nominal length for Fe−N bonds, the average bond length increases.

Starting Model for Refinement of FeSOD. The structure of *E. coli* Fe(III) SOD was initially determined by multiple isomorphous replacement and electron density averaging at 3.1 Å resolution (Stallings et al., 1983). The model was subsequently rebuilt using the structure of *T. thermophilus* MnSOD (Stallings et al., 1985) as a guide and was refined with the Hendrickson−Konnert PROLSQ programs (Hendrickson, 1985) to $R = 0.33$ at 2.5 Å resolution. After incorporation of the sequence deduced from the DNA (Carlioz et al., 1988), model refinement with simulated annealing in X-PLOR reduced R to 0.226 for the 15 219 measurements between 10.0 and 2.5 Å.

X-PLOR Refinement of Fe(III)SOD at High Resolution. Gradual extension of the data from 2.5 to 2.0 Å, with simulated annealing in X-PLOR (Brünger et al., 1990), resulted in a model with $R = 0.227$ (5.0 −2.0 Å, no solvents). Solvents, identified in difference maps, were added to the model and refined with PROLSQ to provide coordinates which served as the starting point for the sequence of X-PLOR computations summarized in Table 2. Step A included 148 cycles of positional refinement and 20 cycles

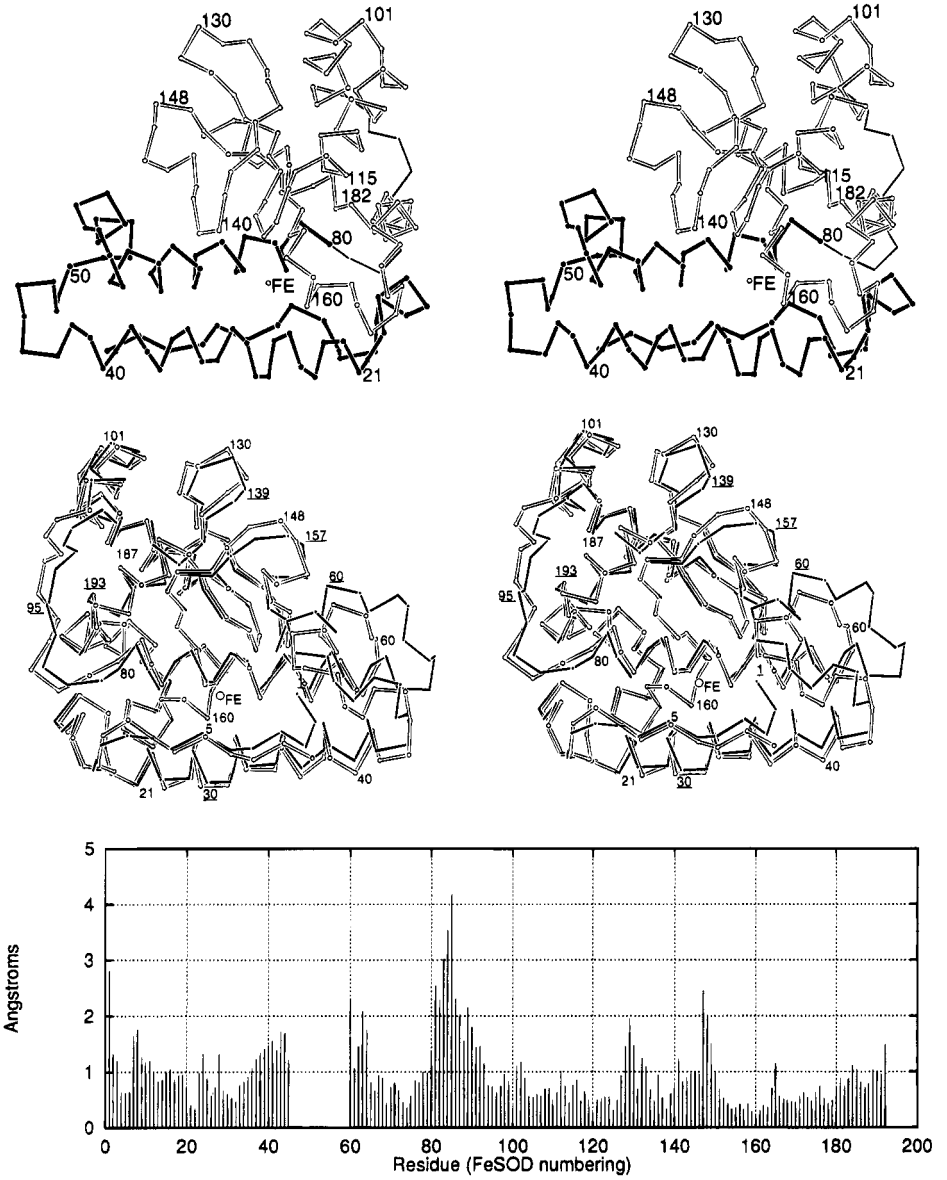

FIGURE 1: (a, top) Stereodrawing of the monomer of *E. coli* FeSOD, oriented to show the division into domains. The amino-terminal domain (residues 1−80, denoted with thick filled bonds) is composed of two long antiparallel α-helices, and the carboxyl-terminal domain (residues 90−192, with shaded bonds) is an α + β structure. The region which varies most among known SODs is to the left, starting near residue 45 (see panel b). Contacts between domains are made by one edge of the β-sheet and its cross-connector (residues near 120, 140−145, and 150−155) with a portion of helix α3 (residues 64−80), by the region near *cis*-Pro16 (residues 14−19) with helix α6 (residues 165−181), and at the Fe−ligand cluster. Residues constituting the hydrophobic core of the domain interface in FeSOD are listed in the text. (b, middle) Superposition of the structures of *T. thermophilus* MnSOD and *E. coli* FeSOD. The structures were aligned by matching the backbone atoms of residues 1−45 and 60−192 from FeSOD with 3−47 and 70−202 from MnSOD. Several of the hydrophobic residues in the domain−domain interface are different in *E. coli* FeSOD and *T. thermophilus* MnSOD: Leu of MnSOD is replaced by Phe at position 75 (FeSOD numbering), Phe by Tyr at 76, and Leu by Cys at 79 in helix α3; Val is replaced by Leu at 153 and Ile by Val at 155 in sheet β3; Ile is replaced by Phe at 177, Val by Leu at 180 and Leu by Val at 181 in helix α6. The insertion of seven residues in MnSOD, starting at position 59 of FeSOD (Figure 2), can be seen in this drawing. (c, bottom) Graph of rms deviations between residues of *E. coli* FeSOD and *T. thermophilus* MnSOD after an alignment (Callahan et al., 1990) that matched all residues except 46−59 of FeSOD and 48−69 of MnSOD. The overall rms deviation of the matched backbone atoms was 1.14 Å. The domain connectors show larger structural divergence than any of the other regions used in the alignment. Residues at the start of helix α3 and residues at two exterior turns in the second domain, near positions 130 and 148 in FeSOD, deviate by about 2 Å.

of refinement of individual atom temperature factors. At step B, the inner resolution cutoff was extended from 5.0 to 40.0 Å, and a bulk solvent correction was applied (Brünger, 1992). After step C the refinement used the data which had been recollected to 1.85 Å resolution from a crystal transferred to pH 7.0 buffer (Table 1). To incorporate the new data, rigid body refinement (step D) was performed starting with the coordinates of step C and was followed by 96 cycles of positional refinement. At step E, low resolution data were again included; ($|2F_o| - |F_c|$) and ($|F_o| - |F_c|$|) maps computed after this step revealed additional solvent molecules. At the conclusion of step F the average B for protein atoms was 12.3 Å^2, compared to an overall B of 12.6 Å^2 derived from Wilson plots of data between 4.0 and 1.85 Å. After step F, coordinates for the metal−ligand cluster were omitted from the model of Fe(III)SOD for 80 cycles of positional refinement in order to compare omit maps with the refined coordinates for the metal and ligand atoms. The densities in the resulting ($|F_o| - |F_c|$) maps corresponded closely to the metal and ligand coordinates obtained in earlier

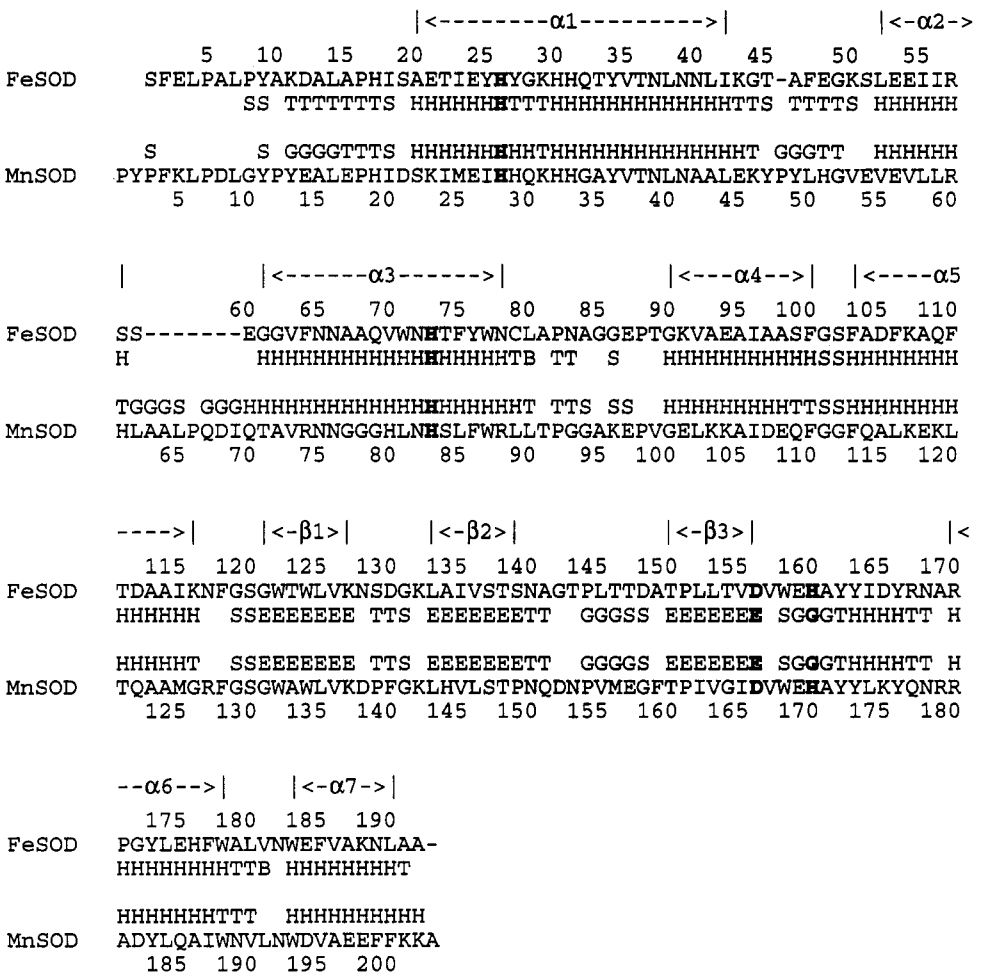

FIGURE 2: Secondary structures in FeSOD from *E. coli* and the structural alignment of *E. coli* FeSOD with *T. thermophilus* MnSOD. Assignments of helices and sheet strands in FeSOD (top lines) are according to Kabsch and Sander (1983), as are the designations of residue conformations in lines 3 and 4. The nomenclature of Kabsch and Sander is followed: H = α-helix; E = sheet strand; T= turn; S = bend; G = 3_{10} helix. The major differences between the *E. coli* FeSOD and *T. thermophilus* MnSOD structures occur between residues 45 and 61 of the FeSOD protein. An inserted loop of seven residues in MnSOD follows position 59 of *E. coli* FeSOD, and a single insert occurs in MnSOD after residue 45 of FeSOD. The alignments of this region given in Ludwig et al. (1991) are different and were based on sequence matching. The legend in that paper incorrectly states that alignment in the variable region beyond position 45 was from the structures.

cycles. The deviations in bond lengths between chains A and B are 0.04 Å and give a minimum estimate of the errors in these parameters.

Refinement of the Reduced Structure, Fe(II)SOD. The structure of Fe(II)SOD was refined starting from the protein model obtained in step C of refinement of oxidized Fe(III)-SOD. The initial R value for data from 5.0 to 2.0 Å resolution and amplitudes greater than $2\sigma(F)$ was 0.305 and decreased to 0.215 after rigid body, positional, and isotropic temperature factor refinement (step A). The solvent ligated to Fe was not included in the refinement at step A (Table 2). Subsequent computation of a difference ($|F_o| - |F_c|$) map revealed electron density corresponding to a coordinated solvent molecule at the axial position in each of the active sites, as in the Fe(III) structure (Figure 6). The remaining steps of refinement included the coordinated solvent molecule. Difference maps computed after step A were used to position 185 solvent molecules from the set of solvents located in the Fe(III)SOD structure at step B. Simulated annealing was conducted in step G to assess the effects of the dynamics and slow-cooling protocols on the metal−ligand geometry (Table 2). The final R factor was 0.188 for all data from 40.0−1.80 Å resolution. The occupancy and temperature factors of metal and coordinated solvent are reported in Table 5.

Refinement of the Fe(III)SOD Azide Complex. The structure of the azide complex was refined starting from the model obtained in step C of refinement of oxidized Fe(III)-SOD. The new data set to 1.8 Å, described in Table 1, was used throughout the refinement. ($|2F_o| - |F_c|$) and ($|F_o| - |F_c|$|) maps calculated after initial refinement in which azide and the solvent ligand were omitted from the atomic model (step A) revealed two peaks adjoining the metal (Figure 7). The coordinated solvent molecule and the azide ligand were included in subsequent refinement and were restrained using force constants of 65.0 kcal/mol·Å^2 for bond lengths and 5.0 kcal/mol·rad^2 for angles. Positional refinement in steps C through H shifted the iron and the in-plane ligands to accommodate the azide ligand. When refinement of the azide occupancies indicated incomplete saturation of the azide site (occupancy factors for azide were 0.45 and 0.67 in the two chains, respectively), the refinement strategy was modified at step I to incorporate alternate conformations for the metal and its ligands. One conformer corresponded to the unligated Fe(III)SOD site as determined by refinement and the second conformer represented the six-coordinate

azide complex. Positional refinement and simulated annealing, with the usual restraints and 0.50 occupancy of each conformer, did not maintain the geometry of the unligated Fe(III) site. Shake restraints (Brünger, 1992) were therefore applied to the Fe(III) conformer during subsequent refinement. This strategy should maximize the differences between the azide complex and the unligated Fe(III)SOD parameters. Occupancy refinements were repeated after the restrained positional refinements (Tables 4 and 5). The final *R* value was 0.186 for all data from 40.0 to 1.80 Å resolution.

Refinement of Mn(III)SOD−Azide. Refinement started with the model of Mn(III)SOD (Ludwig et al., 1991) which resulted from PROLSQ refinement (Hendrickson, 1985). For refinement of the azide complex using X-PLOR, the low resolution cutoff was extended from 10.0 to 20.0 Å, and a bulk solvent correction was applied. With addition of the low resolution data, it was possible to rebuild some of the side chains that were ill-defined in the starting structure, and additional water molecules were located.[1] As with the FeSOD(III)−azide complex, difference maps calculated after rigid body, positional, and *B*-factor refinement omitting nonprotein ligands to Mn (step B in Table 2) clearly showed the locations of the solvent and azide molecules (Figure 8). Refinement proceeded with the inclusion of the solvent and azide molecules. The *R* factor after 135 total cycles of alternating positional and *B*-factor refinement was 0.184 for all data between 20.0 and 1.8 Å. In step D, simulated annealing refinement was conducted with alternate conformations (unligated and azide complex) having equal occupancy, and the unligated Mn(III) geometry was maintained with Shake restraints. As with the FeSOD structures, refinement was concluded with a re-examination of the solvent contribution, resulting in the addition of 15 water molecules.

RESULTS

Structure of E. coli Fe(III)SOD and Comparisons with T. thermophilus MnSOD

The Monomer Fold. The polypeptide chain of Fe(III)-SOD forms a two-domain structure (Figure 1a) with the domains joined by a single extended connector (residues 81−88) that lies on the surface of the molecule. Division of the fold into these two domains is based on distance plots, presented in earlier reports (Stallings et al., 1983; Ludwig et al., 1991). The strong conservation of structure within the Fe- and MnSOD family (Carlioz et al., 1988) is illustrated by the superposition of the monomer chains of *E. coli* FeSOD on *T. thermophilus* MnSOD (Figure 1b,c). Several unusual structural features are duplicated in *E. coli* FeSOD and *T. thermophilus* MnSOD (Ludwig et al., 1991; Stallings et al., 1992): a *cis*-proline (residue 16 in FeSOD) in the turn preceding the first helix, an inserted residue (Gly28 in FeSOD) that alters the geometry of the first helix near the metal ligand, and a characteristic "loop" at the terminus of sheet strand 3 (residues 156−160 in FeSOD), which contributes the third and fourth metal ligands (Figures 1 and 2).

Alignments of the known sequences and three-dimensional structures of Fe- and MnSODs (Carlioz et al., 1988; Chan et al., 1990; Ludwig et al., 1991) indicate that insertions and variations are limited to a few regions of the chain. Major insertions have been observed in one highly variable region, which begins at position 46 in *E. coli* FeSOD. The long helices of the first domain, α1 and α3, are connected by this variable region, which forms a short helix (α2) in *E. coli* FeSOD, *P. ovalis* FeSOD, and MnSODs from *B. stearothermophilus* and *T. thermophilus*, but not in human mitochondrial SODs. In the two known tetrameric MnSOD structures, this part of the chain is involved in the dimer−dimer interactions that stabilize the tetramer (Ludwig et al., 1991; Borgstahl et al., 1992; Wagner et al., 1993). Other variable regions include the external turns that connect the β-sheet strands, and the domain connector, where the positions and interactions of the residues vary from one structure to another (cf. Parker & Blake, 1988).

The Domain (Intrachain) Interface in E. coli FeSOD. The domain interfaces in Fe- and MnSODs are extensive, with areas of about 1100 Å^2 in each of the contact surfaces (Ludwig et al., 1991). Within the interface the contacts are predominantly hydrophobic. Residues at the center of this interface in *E. coli* FeSOD are Leu14, Ile18, Asn72, Phe75, Tyr76, Cys79, Leu80, Trp122, Trp124, Leu153, Val155, Tyr173, Leu174, Phe177, Leu180, and Val181. The domains are also held together by polar interactions, including nine interdomain hydrogen bonds, and are connected by the metal−ligand cluster. Despite a number of residue substitutions, some of which are listed in the legend to Figure 1b, the backbone atoms of the interface residues correspond closely in *E. coli* FeSOD and *T. thermophilus* MnSOD (rmsd = 0.52 Å for the residues in hydrophobic contacts). Residue substitutions do alter the interactions of polar side chains with other main- or side-chain atoms and may affect the stability of the domain interface. Only three of the ten interdomain hydrogen bonds noted in *T. thermophilus* MnSOD (Ludwig et al., 1991) are preserved in *E. coli* FeSOD, but six alternative hydrogen bonds are formed at this interface in the FeSOD structure. Interestingly, the buried hydrogen bonds that position the conserved C-terminal strand, Trp-Asn-Val/Leu-Leu/Val-Trp, against helix α_3 are not identical in the two structures. Salt bridges are not observed in the FeSOD interface: the bridge between Arg74 and Asp152 in *T. thermophilus* MnSOD is lost by the substitution of Phe64 and Gly142 in FeSOD, and the bridge between Arg88 and Glu198 in MnSOD has no equivalent in FeSOD. The possible role of salt bridges in conferring thermal stability on proteins from thermophiles like *T. thermophilus* has been discussed (Menendez-Arias & Argos, 1989; Davies et al., 1993)

The Monomer−Monomer (Interchain) Interfaces and the Substrate Funnels in FeSOD and MnSOD. A characteristic monomer−monomer interface forms around the local dyad in all of the Fe- or MnSOD structures which have been determined by X-ray methods (Ringe et al., 1983; Stallings et al., 1983, 1985; Parker & Blake, 1988; Stoddard et al., 1990a; Borgstahl et al., 1992; Wagner et al., 1993). This interface, about 1000 Å^2 in area, is more highly conserved than the domain−domain interface. For 13 identical interface residues in *E. coli* FeSOD and *T. thermophilus* MnSOD,

[1] The improvement in the model of the azide complex resulting from inclusion of the innermost data prompted us to refine the Mn(III)SOD model with data between 20.0 and 1.8 Å. A total of 440 cycles of refinement using X-PLOR were performed, alternating positional and *B*-factor adjustment. The beginning and final *R* factors were 0.202 and 0.187, respectively.

Table 3: Conservation of Dimer Interfaces in Fe- and MnSODs. RMS Deviations in Positions after Alignment of *E. coli* FeSOD and *T. thermophilus* MnSOD

residue (FeSOD numbering)	rms distance (Å)[a] (backbone)	rms distance (Å) (side chain)
Tyr 25 (Ile)	0.62	
Lys 29	0.66	1.78
His 30	0.41	0.27
Tyr 34	0.42	0.29
Asn 65	0.58	0.76
Phe 118	0.36	0.62
Gly 119	0.24	
Ser 120	0.12	0.12
Asn 140	0.54	0.55
Ala 141 (Gln)	1.15	
Trp 158	0.23	0.28
Glu 159	0.11	0.14
His 160	0.12	0.14
Tyr 163	0.40	0.28
Ile 164 (Leu)	0.74	
Arg 167 (Gln)	0.60	
Asn 168	0.56	1.64

[a] Overall RMS deviation of backbone atoms of 17 interface residues is 0.53.

the rms deviation of all atoms is 0.61 Å (Table 3). Seventeen solvents (including local symmetry mates) that are part of the structure of the interface in FeSOD are duplicated in *T. thermophilus* MnSOD (Ludwig et al., 1991). The dimer interface of *E. coli* Fe(III)SOD is shown in Figures 3 and 4a. The principal monomer−monomer contacts are made by residues at the termini of the three sheet strands and by residues from helix α1. Altogether, the interactions at this interface in *E. coli* FeSOD involve 17 residues from each chain. At the center of the dimer interface of *E. coli* FeSOD, Ser120 is hydrogen-bonded to its local symmetry mate as in other Mn- and FeSOD dimers. The side chains of Glu159 cross the interface, with OE1 of Glu159 from one chain hydrogen bonding to the amide nitrogen of Glu159 from the second chain; additional interchain hydrogen bonds are formed between Glu159 and His160, and between His30 and Tyr163.

The monomer−monomer packing generates two symmetry-related funnels that lead from bulk solvent toward the metal ions. As illustrated in Figure 4a, the axes of these substrate funnels are approximately perpendicular to the 2-fold axis relating the monomer chains. The linings of the funnels are formed primarily by residues from helices α1 and α3 of one chain and residues from helix α5 of the other chain (Figure 4). In *E. coli* FeSOD 11 residues from the A chain and eight from the B chain contribute atoms that are exposed to solvent in the funnel. At the vertex of the funnel, residues His30 and Tyr34 block access to the metal. Computations indicate that omisson of the Tyr34 side chain allows access of substrate to the metal, suggesting that this residue may move to permit the passage of inner sphere ligands (Sines et al., 1990). In agreement with computations of electrostatic effects that point to a functional role for basic residues of the funnel (Bacquet et al., 1988), modification of the residue equivalent to Arg170, which is at the funnel entry in *E. coli* FeSOD, decreases the rate of the second-order reaction with O_2^- in several Mn- and FeSODs (Chan et al., 1990). The conservation of residues at the dimer interface (see above) also preserves many of the features of the substrate funnel. Only two of the residues depicted in Figure 4b, Lys115 and Ile116, are replaced in *T. thermophilus* MnSOD, where the equivalent residues are Gly and Met.

Metal Selectivity. The selectivity of many SOD proteins for either Fe or Mn (Ose & Fridovich, 1979) is curious in view of the structural similarities displayed by these proteins and is not well-understood. It has been suggested that metal specificity may be associated with residue substitutions at critical sites, and this idea has been examined by comparisons of proteins that are selective for iron or manganese. The most striking variation revealed by sequence alignments is the location of the glutamine whose side chain is at the center of the hydrogen bonding network in the metal-binding site (Chan et al., 1990). This Gln is part of helix α3 in iron proteins but participates in a turn between sheet strands in manganese-specific proteins; the distance between equivalent Cα atoms at these locations is ~5.5 Å. Nevertheless, the Gln side chain amide occupies very similar positions in the structures of *E. coli* FeSOD and *T. thermophilus* MnSODs (see Figure 10). Other residues that appear to be characteristic of FeSODs are Trp71 and Phe75, at the domain−domain interface in the vicinity of the metal-binding site. Their substitution by the Leu residues characteristic of MnSOD does not appear to distort the domain interface in this region. Thus the present comparisons of the high resolution structures of *E. coli* FeSOD and *T. thermophilus* MnSOD do not offer any obvious clues to metal specificity.

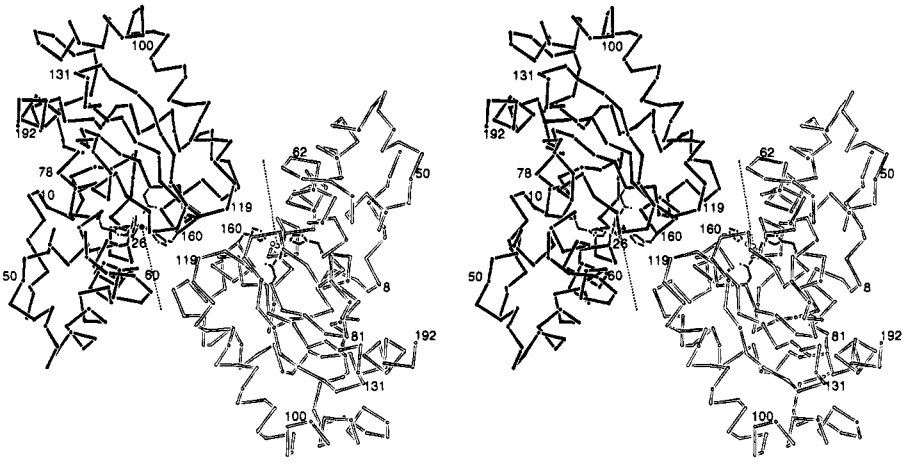

FIGURE 3: Stereodrawing of dimeric FeSOD from *E. coli*. The Cα representation of the dimer is viewed down the local 2-fold axis of the molecule. The four protein ligands of Fe are drawn in full-atom representation. Dotted lines showing the presumed direction of substrate approach are included to indicate the orientation of the substrate funnels with respect to the local symmetry (cf. Figure 4.)

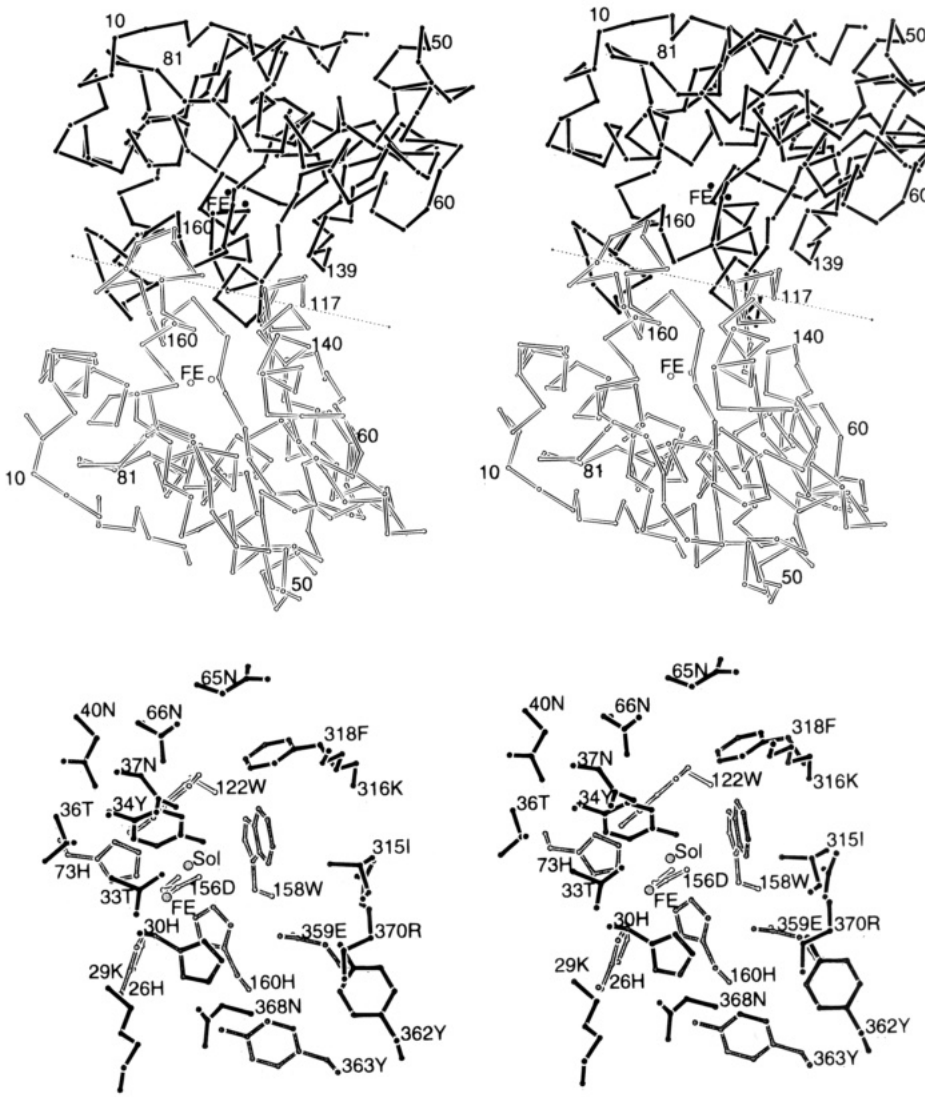

FIGURE 4: Stereoviews of the substrate funnel in FeSOD, approximately along one of the funnel axes depicted in Figure 3. (a, top) Overview of the way in which both chains of the dimer participate in formation of the substrate channel. The A chain is represented by solid bonds. This view shows clearly how residues from helices α1 and α3 of chain A and α5 of chain B contribute to the outer opening of the funnel. The position of the 2-fold axis is indicated for reference (dotted line). (b, bottom) Details of the substrate funnel leading to the active site of chain A, viewed in the same direction as in the top panel but rotated 90° so that the residues from the B chain are to the right (the numbering of B chain residues begins at 201). The outermost entry of the funnel is formed from Arg170, Ile115, and Lys116 of the B chain, along with Thr33, Asn37, Asn65, and Asn66 of the A chain. Moving toward the metal, the next layer of side chains includes Lys29A, Phe118B, Tyr162B, and Asn168B. The innermost residues are His30A, Tyr34A, Glu159B, and Tyr163B.

Characteristic residue exchanges do not seem to be associated with significant alterations in the folded structure in the vicinity of the metal binding site, the substrate entry funnel, or the dimer interface. Examination of the unselective SODs that form active enzymes by binding either Fe or Mn (cambialistic SODs) likewise fails to pinpoint a basis for metal selectivity (Matsumoto et al., 1991).

If the incorporation of metals is dependent on closure of the domains during folding, as suggested elsewhere (Ludwig et al., 1986), then the observed differences in the domain connectors and in interdomain interactions might influence the recognition and incorporation of metals. A role for accessory proteins in metal incorporation cannot be excluded.

Metal−Ligand Interactions

The Metal Binding Site of Fe(III)SOD. The iron is pentacoordinate, with the metal ligands arranged in distorted trigonal bipyramidal geometry (Table 4 and Figure 5). Three of the four protein ligand atoms, NE2 of His73, OD1 of Asp156, and NE2 of His160, form the trigonal basal plane, and the fourth, NE2 of His26, is coordinated at one axial position. A solvent *trans* to the axial histidine ligand completes the distorted trigonal bipyramid (Table 4). The presence of solvent ligands in *E. coli* FeSOD and *T. thermophilus* MnSOD has been verified by omit refinements (Materials and Methods; Ludwig et al., 1991). Occupancies of the solvent sites refine to values near 1.0 in the crystallographically independent chains of *E. coli* FeSOD (Table 5).

The metal−ligand bond distances are in the range observed in many model compounds (Rardin et al., 1991). The Fe(III)−nitrogen bond distances vary from 2.03 to 2.17 Å, with the axial bond tending to be longer than the in-plane bonds, and the average Fe(III)−OD1 156 and Fe(III)−O 194 distances are 1.91 and 1.96 Å. In independent EXAFS measurements (Tierney et al., 1995), the average Fe(III)−ligand bond distance is found to be 1.98 Å, matching closely the value of 2.03 Å derived from the refinements reported

Table 4: Metal Coordination Geometry[a]

	oxidized Fe(III)SOD	reduced Fe(II)SOD	azide–Fe(III)SOD		oxidized Mn(III)SOD	azide Mn(III)SOD
bond lengths (Å)				bond lengths (Å)		
Fe–NE2(26)	2.16	2.18	2.21	Mn–NE2(28)	2.15	2.12
Fe–NE2(73)	2.05	2.04	2.13	Mn–NE2(83)	2.10	2.07
Fe–OD1(156)	1.91	1.94	2.03	Mn–OD1(166)	1.80	2.25
Fe–NE2(160)	2.07	2.12	2.15	Mn–NE2(170)	2.18	2.12
Fe–OH2(194)	1.96	2.04	2.00	Mn–OH2(205)	2.09	1.95
Fe–NA1			2.12	Mn–NA1		2.22
average	2.03	2.06	2.11	average	2.06	2.10
bond angles (deg)				bond angles (deg)		
NE2(26)–Fe–NE2(73)	94.84	95.29	96.13	NE2(28)–Mn–NE2(83)	92.52	92.85
NE2(26)–Fe–OD1(156)	85.18	84.96	83.30	NE2(28)–Mn–OD1(166)	87.67	83.12
NE2(26)–Fe–NE2(160)	90.52	92.47	89.53	NE2(28)–Mn–NE2(170)	90.62	91.04
NE2(26)–Fe–OH2(194)	171.89	171.89	171.10	NE2(28)–Mn–OH2(205)	171.89	169.84
NE2(73)–Fe–OD1(156)	112.33	112.85	94.95	NE2(83)–Mn–OD1(166)	110.44	106.12
ME2(73)–Fe–NE2(160)	127.94	126.58	160.78	NE2(83)–Mn–NE2(170)	131.16	147.59
OD1(156)–Fe–NE2(160)	119.72	120.46	103.48	OD1(166)–Mn–NE2(170)	118.38	106.16
NE2(26)–Fe–NA1			96.45	NE2(28)–Mn–NA1		107.78
NE2(73)–Fe–NA1			85.74	NE2(83)–Mn–NA1		73.46
OD1(156)–Fe–NA1			171.89	OD1(166)–Mn–NA1		168.87
NE2(160)–Fe–NA1			75.65	NE2(170)–Mn–NA1		74.92
Fe–NA1–NA2			117.04	Mn–NA1–NA2		143.24
NA1–NA2–NA3			171.89	NA1–NA2–NA3		168.87

[a] Target values for the angles in the azide complexes were as follows: N(His73/83)–Me(III)–N(His160/170), 150°; N(His73/83)–Me(III)–O(Asp156/166), 100°; O(Asp156/166)–Me(III)–N(His160/170), 100°.

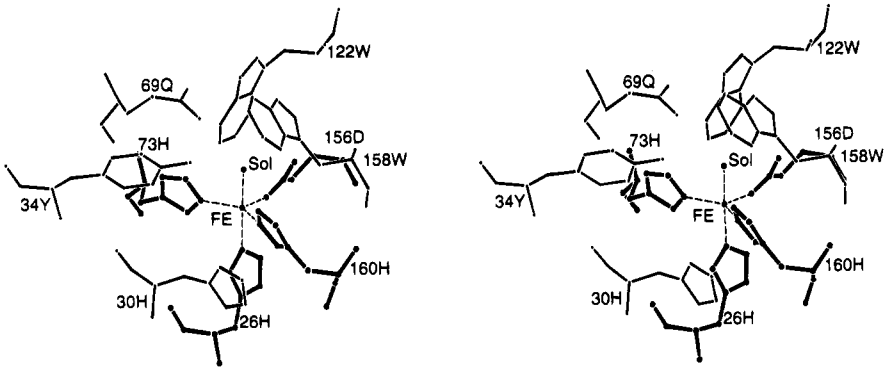

FIGURE 5: Metal–ligand geometry and the environment of the metal–ligand cluster in FeSOD. The view is approximately perpendicular to the axis of the trigonal bipyramid formed by the five Fe ligands and shows the open face of the cluster, between the rings of His73 and 160. Imperfect packing at this coordination site leaves a cavity (Stallings et al., 1991, 1992) which may assist ligation of substrate (see Figure 8c). Bond lengths and angles are listed in Table 4.

here. The ligand–Fe–ligand angles for the axial ligands are near to the values of 180° and 90° expected for trigonal bipyramidal geometry. Distortions arise primarily from deviations of the bond angles in the trigonal basal plane. The two angles, 73NE2–Fe(III)–160NE2 and 73NE2–Fe(III)–156OD1, are 128° and 112°, 8° from the ideal value of 120°. Thus the observed geometry is much closer to an ideal trigonal bipyramid than to a square pyramid. The planes of the imidazole rings of His73 and His160 are almost perpendicular to the trigonal plane defined by the metal ligands. The orientation of these imidazole rings, combined with distortion in the ligand–Fe–ligand angles, permits approach of an additional ligand *trans* to the OD1 of Asp156.

The geometry at the metal center of Fe(III)SOD can be compared not only with MnSOD from *T. thermophilus* (Table 4) but also with the models for *B. stearothermophilus* MnSOD (Parker & Blake, 1988), for human MnSOD (Borgstahl et al., 1992; Wagner et al., 1993), and for *P. ovalis* FeSOD (Stoddard et al., 1990a). The arrangement of protein ligands in *E. coli* FeSOD is very similar to that in *B. stearothermophilus* MnSOD, human MnSOD, and *T. thermophilus* MnSOD. In contrast, the ligand–metal geometry reported for FeSOD from *P. ovalis* is much more distorted from the ideal trigonal bipyramid. The iron is displaced from the trigonal plane, and the Fe–axial N bond length is 2.6 Å. The basis for these apparent differences in the protein–metal coordination in *P. ovalis* FeSOD is not clear but may be related to some instability of the metal center at low pH (Fee et al., 1981). Solvents ligated to Fe or Mn have not been located in the models of MnSOD from *B. stearothermophilus* (Parker & Blake, 1988) or in FeSOD from *P. ovalis* (Stoddard et al., 1990a). A solvent ligand is included in the structure of human MnSOD (Borgstahl et al., 1992) which was determined by molecular replacement using *T. thermophilus* MnSOD as a search model.

The Fe(II) SOD Structure. Maps calculated after an initial refinement that omitted all solvents (step A of Table 2) revealed a peak ($>10\sigma$) at the position of the solvent ligand, indicating the retention of this ligand in the Fe(II) enzyme (Figure 6). The average Fe–ligand bond length increases slightly on reduction (as expected from the increased target values), but the bond angles do not change significantly

Table 5: Occupancies and Thermal Parameters

		chain A		chain B	
		occupancy	B (Å^2)	occupancy	B (Å^2)
Fe(III)SOD[a]	metal	1.00	5.24	1.00	5.65
	solvent	1.00	3.78	1.00	8.89
Fe(II)SOD	metal	1.00	4.27	1.00	5.50
	solvent	1.00	6.79	0.98	8.08
Fe(III)SOD−azide	metal	0.99	6.92	1.03	8.91
	solvent	0.99	7.47	1.03	10.16
	azide	0.48	7.06	0.50	5.82
		0.48	7.98	0.50	4.71
		0.48	5.82	0.50	4.29
Mn(III)SOD	metal	0.97	7.17	0.97	7.33
	solvent	1.00	6.79	0.98	6.91
Mn(III)SOD−azide	metal	1.03	7.94	1.05	8.52
	solvent	1.03	7.07	1.05	8.83
	azide	0.51	9.94	0.50	12.11
		0.51	12.96	0.50	14.95
		0.51	15.30	0.50	16.55

[a] Two modes of occupancy refinement were tested with data for Fe(III)SOD; in one case initial occupancies of the metal and coordinated solvent were set to 1.0 and in the other the initial occupancies were 0.5.

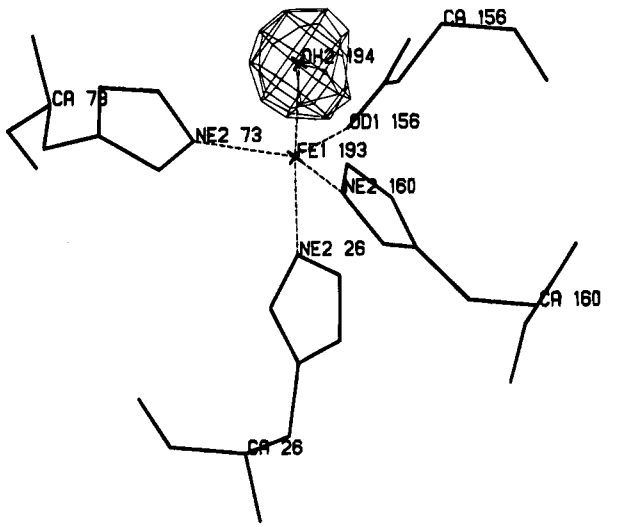

FIGURE 6: Omit ($|F_o| - |F_c|$) map showing density corresponding to the solvent ligand in Fe(II)SOD. Phases were from step A of Table 2 ($R = 0.215$ with no solvents). Contours are drawn at 3σ; the peak maximum is approximately 9σ.

(Table 4). Reduction of Fe(III)SOD by addition of dithionite to crystals is not associated with any major changes in the protein structure. After a round of simulated annealing with the data from Fe(II)SOD (step G of Table 2) and inspection of the solvents, the rms deviation of the Cα atoms of the Fe(III)SOD and Fe(II)SOD structures is only 0.09 Å.

The Azide Complex of Fe(III)SOD. Azide occupies a cavity bounded by the ring of His73 and the backbone of His30. The azide NA1 bonds to iron in-plane at the open face between His73 and His160 (Figures 7 and 8). Difference maps computed after refinements omitting both azide and solvent ligands show the azide density and another nonoverlapping peak that corresponds to a solvent molecule in the same position as in Fe(III)SOD (Figure 7). The occupancies estimated by refinement indicate that iron simultaneously coordinates both ligands (Table 5). Ligation of azide ion, without dissociation of the bound solvent molecule, increases the coordination number of the metal center from five to six. The other bonds elongate slightly when azide is bound; the average metal−ligand bond distance for the six ligands is 2.11 Å. EXAFS studies of the azide complex of *E. coli* FeSOD determine an average metal-ligand bond distance of 2.07−2.08 Å (Tierney et al., 1995).

The geometry of the six-coordinate azide complex is distorted octahedral[2] (Table 4). Coordination of azide *trans* to the OD1 of Asp156 produces some structural perturbations in the active site environment (Figure 7). Because azide was not bound to every molecule in the crystal and two conformations had to be accommodated in the refinements, the angles that characterize the azide complex are not as well-determined as those for unligated Fe(III)SOD. Refinements in which the geometry of the unligated fraction of the structure was restrained to be close to that found in the Fe(III)SOD structure (see Materials and Methods) indicate that insertion of azide increases the bond angle at 73NE2−Fe(III)−160NE2 by more than 30°, to 162°. The Fe shifts slightly (0.20 Å toward the azide nitrogen) and the phenol oxygen of Tyr34 moves away from the metal center by 0.44 Å. Movement of the imidazole ring of His73 increases the angle between the ring plane and the NE2−Fe bond (Figure 7). Changes elsewhere in the structure are minimal. At the conclusion of refinement, the rms difference between the Cα atoms in Fe(III)SOD and Fe(III)SOD−azide is 0.11 Å.

Spectroscopic and kinetic data furnish evidence for more than one mode of azide binding by FeSOD. Azide interacts with Fe(III)SOD in a two-step process with an overall K_d of 1−2 mM (Fee et al., 1981; Bull & Fee, 1985). Only the second step is accompanied by changes in the visible absorbance of Fe(III), implying the existence of an additional "pocket" for initial binding of azide. Inhibition by anions like perchlorate is also observed in the absence of spectral changes and has been attributed to binding at or near the secondary site for azide (Bull & Fee, 1985). It is tempting to suggest that this site is near Tyr34 and His30 at the vertex of the substrate funnel. In the high salt media employed for crystallization the K_d for azide appears to increase (Fee, unpublished observations). We assume that the complex observed in the crystals, with azide coordinated to Fe, corresponds to the final species detected in the kinetic studies of azide binding, but we find no evidence for a second bound azide even at azide concentrations of 100 mM. The structure does not offer a ready explanation for the dramatic effect of azide on solvent proton relaxation by Fe(III)SOD (Dooley et al., 1987).

The Azide Complex of Mn(III)SOD and Comparisons with the Azide Complex of Fe(III)SOD. The refined structure of the azide complex of Mn(III)SOD from *T. thermophilus*, based on data from 20.0 to 1.8 Å resolution, shows azide coordinated to Mn(III) at an in-plane site opposite to the Asp oxygen ligand, and the His83NE2−Mn−His170NE2 bond angle opened from 131° to 148°. As in the Fe(III)-SOD complex, the axial solvent ligand and azide are bound simultaneously (Table 5). Although the Mn- and Fe-liganded

[2] X-ray data for an azide complex of *P. ovalis* FeSOD have been collected to 2.9 Å from cross-linked crystals and interpreted with a model which places the azide ligand in a site corresponding approximately to the position of the solvent ligands shown in Figures 7 or 8. (Stoddard et al., 1990b). The model incorporates no coordinated solvents and thus includes only five ligands to iron; the geometry is distorted from trigonal bipyramidal with a His26−Fe distance of 3.0 Å.

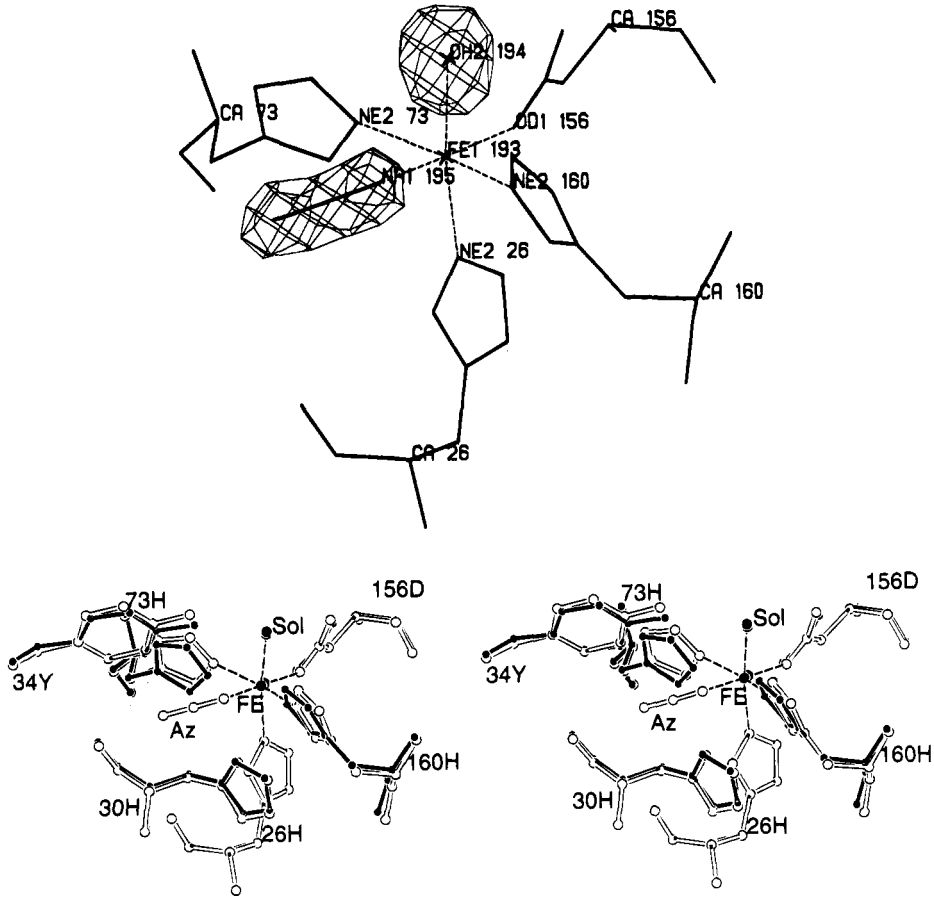

FIGURE 7: Azide complex of Fe(III)SOD. (a, top) An ($|F_o| - |F_c|$) map computed after refinement vs data from the FeSOD−azide complex, starting with a model omitting azide and solvent (step A of Table 2). Positive contours are drawn at 3σ. The peak of the difference density at azide is 7σ and at solvent is 10σ. Coordinates are from the final round of refinement (round J of Table 2). (b, bottom) Stereoview comparing the refined structures of Fe(III)SOD and the azide complex of Fe(III)SOD. The azide complex is drawn with thick open bonds; coordinates for the unligated Fe(III)SOD (thin filled bonds) are from the separate refinement of the Fe(III)SOD structure. Complex formation is accompanied by small displacements of Fe to the left (0.20 Å) and of the imidazole ring of His73 to the right, which open the bond angle NE2 His73−Fe−NE2 His160.

nitrogens of the azide ions are in essentially the same positions in the two structures, the other MnSOD−azide interactions are different from those observed in the azide complex of FeSOD (Figure 8). In MnSOD, the azide ligand adjoins the ring of His170 and points toward the substrate-entry channel, hydrogen bonding to the hydroxyl group of Tyr36. The X-ray data do not show evidence of two modes of azide binding to Mn in MnSOD: the pocket occupied by distal azide nitrogens in FeSOD is free of difference density in maps of the MnSOD−azide complex. The distal nitrogen atoms of azide do have larger temperature factors than the proximal nitrogen bound to Mn, suggesting some mobility of the bound azide.

Whittaker and Whittaker (1991) provided the first definitive evidence for ligation of azide to Mn in Mn(III)SOD. Their spectroscopic measurements on *E. coli* MnSOD showed that azide binds more weakly to Mn(III)SOD than to Fe(III)SOD, with a K_d of approximately 7 mM. However, they found that dramatic changes in the low temperature MCD spectrum were associated with binding of azide by MnSOD, indicating changes in symmetry at the metal site. Whittaker and Whittaker proposed that ligation of azide entails pseudorotation of a distorted five-coordinate species toward square pyramidal geometry, whereas we observe a six-coordinate species with azide oriented differently than in Fe(III)SOD−azide.

DISCUSSION

The refined high-resolution structures of Fe(III)SOD, Fe(II)SOD, and the azide complexes of both Mn(III) and Fe(III)SOD provide details of the metal−ligand coordination in each of these species and furnish the basis for a reaction scheme that postulates inner-sphere electron transfer in both the reductive and oxidative half-reactions.

Any proposed structure-based mechanism for catalysis by FeSOD should account for the following thermodynamic, kinetic, and spectroscopic observations: (1) Ionizations occur with pK_{app} of ~5 and ~9 that are intimately associated with the ferric ion (Fee et al., 1981). As discussed below, these processes are unlikely to be associated with the protein ligands to the metal (histidine and aspartate) but are reasonably assigned to the protonation of a coordinating OH^- (pK_{app} ~5) and to the addition of a second OH^- to the Fe(III) coordination shell (pK_{app} ~9), i.e.

$$\text{Fe(III)}-\text{OH}_2 \rightarrow \text{Fe(III)}-\text{OH}^- + \text{H}^+ \qquad pK \sim 5$$

$$\text{Fe(III)}-\text{OH}^- + \text{OH}^- \rightarrow \text{Fe(III)}(\text{OH}^-)_2 \qquad pK \sim 9$$

(2) One proton (1.1 ± 0.1) is taken up by the protein when it is reduced to the Fe(II) species in the pH range 7−10 (Bull & Fee, 1985). Proton uptake requires a unique basic group

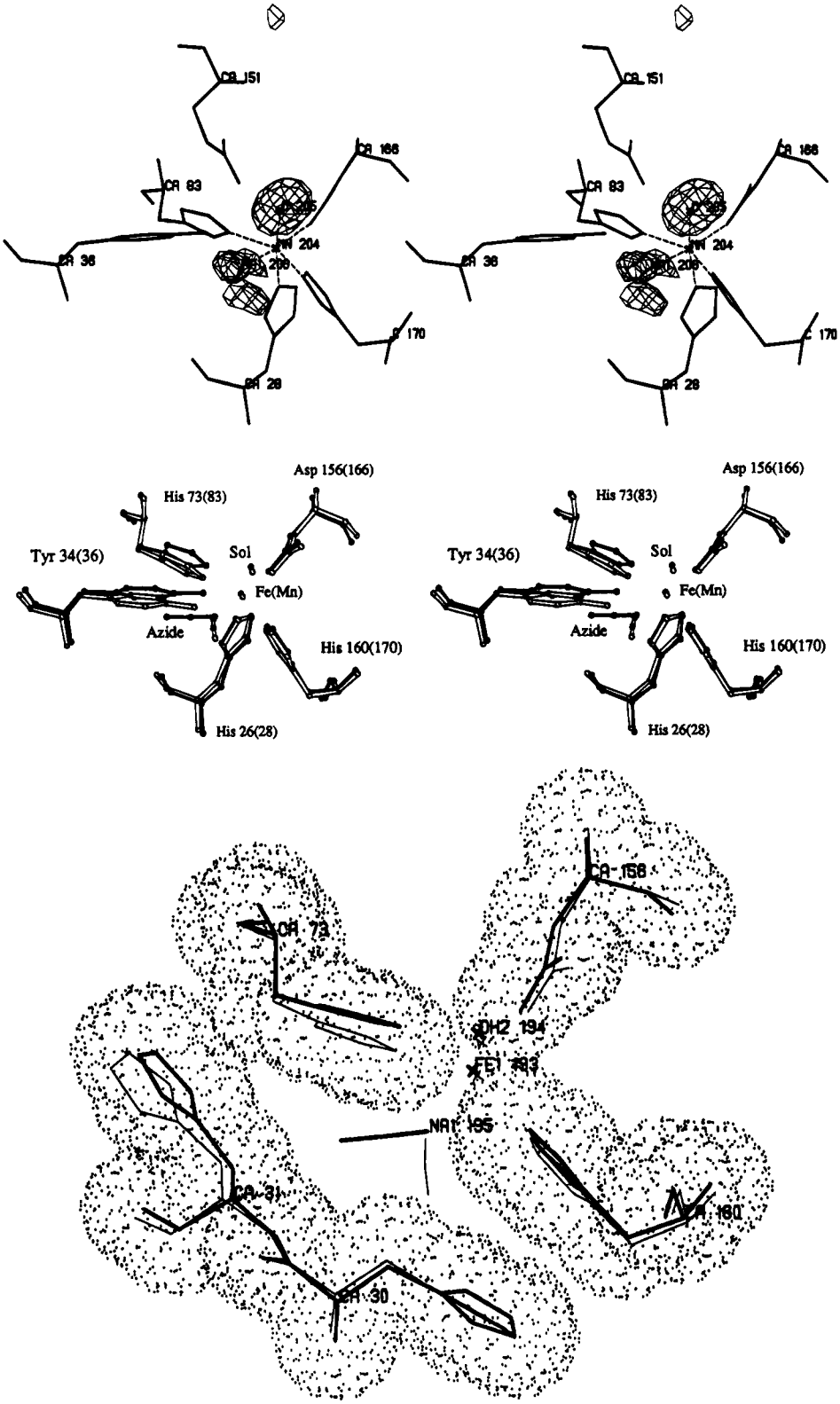

FIGURE 8: Azide complex of Mn(III)SOD. (a, top) Stereoview of an ($|F_o| - |F_c|$) map computed after refinement vs data from the MnSOD–azide complex, starting with a model omitting azide and solvent (step B of Table 2). Positive contours are at 2.5σ. The density closest to the viewer resides at the vertex of the substrate funnel. Coordinates are from the final round of refinement (round E of Table 2). (b, middle) Stereodrawing comparing the azide complexes of Mn(III)SOD (open bonds) and Fe(III)SOD (filled bonds), showing the differences in the orientation of the azide ligand in the two structures. The structures were overlaid using the metals and the six ligand atoms [prepared with the program MOLSCRIPT (Kraulis, 1991)]. (c, bottom) Drawing showing the packing of Fe(III)SOD in the vicinity of the azide binding sites. The thick bonds depict the azide complex of Fe(III)SOD and the thin bonds the azide complex of Mn(III)SOD. Residue numbers refer to the FeSOD structure (see Figure 2). The surface dots represent van der Waals radii of the atoms of azide-free Fe(III)SOD. The models were aligned as in panel b.

(pK > 11) in the ferrous form of the protein *and* a unique acidic group (pK < 6) in the ferric form. (3) As determined by Mössbauer spectroscopy (Niederhoffer et al., 1987), ligands associated with the ferrous ion do not ionize in the

pH range 7−10.8, and the ligation to Fe(II)SOD is unchanged over this range of pH. (4) The apparent Michaelis constant (K_m) for O_2^- is influenced by the pK_a of ~9 in the ferric form and by an ionization in the reduced protein (also at pK_{app} ~9) that is not associated with the metal [cf. Figure 4 of Bull and Fee (1985)]. Finally, (5) the turnover constant (TN) is independent of pH in the range 7−11 and is determined at all pHs by proton transfer from a general acid (most probably water).

The 5−6−5 Mechanism. In Figure 9 we present a scheme [modified from Bull and Fee (1985) and Stallings et al. (1992)] which seems to account for the extant kinetic, spectroscopic, and structural observations of both the oxidized and reduced forms of the protein. A key postulate of the mechanism is that superoxide transiently forms a coordinate covalent bond with the Fe(III) and Fe(II) forms of the metal. For the reductive step [Fe(III) + O_2^- → Fe(II) + O_2], the coordination of azide, as observed by X-ray crystallography, is taken as a model for superoxide binding to Fe(III)SOD. We also assume that in the oxidative step [Fe(II) + O_2^- + $2H^+$ → Fe(III) + H_2O_2], O_2^- binds to Fe(II) prior to inner-sphere electron transfer. Reduction of O_2^- to form the doubly charged peroxide anion is likely to require direct ligation to the metal (Fee et al., 1986). Although neither azide nor OH^- has significant affinity for Fe(II)SOD (Bull & Fee, 1985), NO• does form a stable complex with Fe(II)SOD (Niederhoffer et al., 1987), indicating that a coordination position is available on the reduced metal. In the scheme of Figure 9, the coordination number increases to 6 and returns to 5 in each of the half-reactions. We therefore call this the 5−6−5 mechanism.

Structure refinement with high-resolution X-ray data shows that coordination of azide is accompanied by a shift to distorted octahedral geometry that involves opening the bond angle at 73NE2−Fe−170NE2 by as much as 30°. The atomic displacements of the iron ligands that occur as a result of azide binding vary from <0.1 to 0.6 Å (Figure 7). Formation of Fe(III) inner sphere complexes is thus associated with relatively small reorientations of the metal and its ligands. Reduction to the Fe(II) form produces virtually no changes in structure, relative to the five-coordinate Fe(III)-SOD. The minimal perturbations required to form these catalytic intermediates are consistent with rapid turnover [~26 000 s^{-1} at 25 °C for FeSOD (Bull & Fee, 1985)]. Occupation of the preformed cavity adjoining His30 (Figure 8) would be expected to favor the coordination of substrate (Eriksson et al., 1992), although some expansion of the open region between His30 and His73 is required to bind azide. As noted elsewhere (Sines et al., 1990; Stallings et al., 1992) the binding site for azide is not directly accessible to solvent, and ligands reach the iron only because thermal motions of Tyr34, His 30, or other residues provide a transient pathway.

Proton Uptake and the Protonation States of Intermediates. An OH^- metal ligand in Fe(III)SOD is proposed as acceptor of the proton which is bound when the protein is reduced to Fe(II)SOD. Because a proton acceptor might be expected to be close to the metal ion, where its pK could be influenced by the change in charge on the metal, the metal ligands are prime candidates for this functional role. However, the X-ray structures suggest that none of the four protein ligands is a likely proton acceptor. Asp156 is presumably ionized at pH 7, and the hydrogen-bonding interactions of imidazole residues 26, 73, and 160 (Table 6) indicate that these

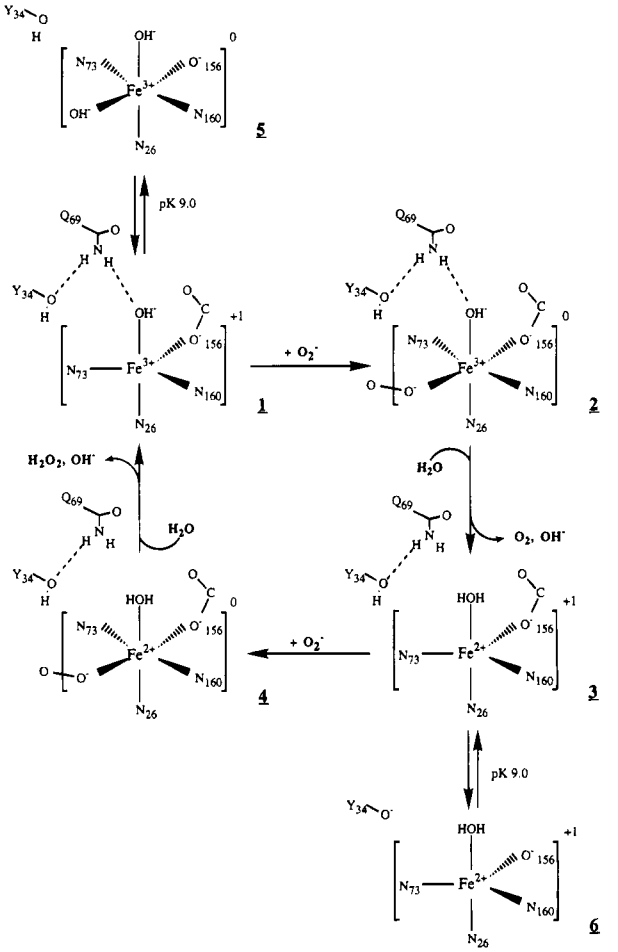

FIGURE 9: Scheme for the enzyme-catalyzed dismutation of superoxide. The geometries for the first three central species have been determined by X-ray analyses. (1) Fe in the resting oxidized enzyme coordinates an axial solvent ligand, postulated to be OH^- at neutral pH. (2) Superoxide anion binds at the partly open coordination site *trans* to OD2 of Asp156 without substitution of ligated hydroxide anion, forming a distorted octahedron. This intermediate is modeled by the azide complex of Fe(III)SOD. Subsequent electron transfer generates the dioxygen leaving group. (3) Protonation of the axial solvent ligand restores the net +1 charge on the cluster for the start of the second half reaction. Free reduced enzyme with trigonal bipyramidal coordination then accepts a second superoxide. (4) The coordinated superoxide anion is reduced and receives two protons, one shown as coming from the ligated HOH molecule, and leaves as hydrogen peroxide, with SOD returning to the resting state (1). Reduction of Fe(III)SOD at high pH (converting species 5 to species 6) would occur with protonation of the axial ligand, loss of the basal OH^- ligand (with accompanying protonation) and ionization of Tyr34. In this scheme, the pK near 9.0 which has been observed in static epr or visible titrations (Slykhouse & Fee, 1976; Fee et al., 1981) of Fe(III)SOD corresponds to formation of species 5, in which a second OH^- ligand is bound at the sixth coordination site. This same pK accounts in part for the pH dependence of the K_m (Bull & Fee, 1985). Mössbauer spectra show that Fe(II)SOD does not change ligation between pH 7 and 11 (Niederhoffer et al., 1987; Bull & Fee, 1985). Therefore the pK near 9.0 in Fe(II)SOD must be assigned to some other group, which we propose is Tyr34 in Fe(II)SOD (species 6).

imidazole ligands are uncharged at neutral pH. Protonation of the Asp ligand or of neutral His ligands would therefore dissociate those ligands from the metal as is observed in Cu/Zn SOD (Bertini et al., 1985). In fact, the protein ligands move only slightly when the protein is reduced to the Fe(II) form (Tables 4 and 6). In contrast, the solvent ligand could accept a proton if it were OH^- rather than HOH. To account for the observed proton uptake, the pK of the solvent [HOH]

Table 6: Polar Interactions of the Metal–Ligand Cluster

atom	residue	atom	residue	Fe(II) SOD distance (Å)	Fe(III) SOD–azide distance (Å)	Fe(II) SOD distance (Å)	Mn(III) SOD distance (Å)	Mn(III) SOD–azide distance (Å)
ND1	His 26/28	O	water	2.79	2.79	2.76	2.64	2.71
OH	Tyr 34/36	O	water	2.76	2.79	2.76	2.72	2.66
		NE2	Gln 69/151	3.14	3.04	3.11	3.05	3.13
O	Gln 69/151	ND1	His 73/83	2.76	2.74	2.74	2.73	2.70
OE1	Gln 69/151	NE1	Trp 122/132	3.09	3.10	3.08	2.94	2.92
OD2	Asp 156/166	O	Wat 194/205	2.96	3.02	2.89	2.76	2.85
ND1	His 160/170	OE2	Glu 359/459	2.96	2.88	2.93	2.79	2.78

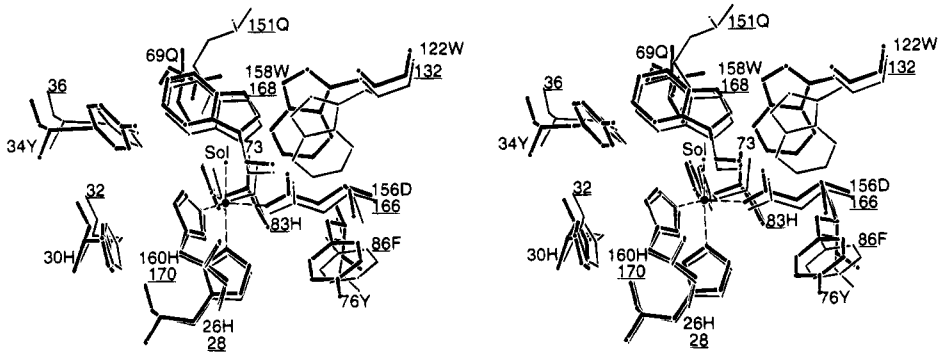

FIGURE 10: Stereoview comparing the active sites of MnSOD from *T. thermophilus* (thinner lines) and FeSOD from *E. coli* (thicker lines). The hydrogen-bonding network involving Gln151 (or 69), ligated solvent, and Tyr36 (or 34) is retained in both structures. This view is rotated approximately 90° from that of Figure 5. Hydrogen-bonding interactions are listed and compared in Table 6.

bound to iron must shift from below pH 6 in Fe(III)SOD to above pH 11 in Fe(II)SOD. These pK values are compatible with the known properties of model Fe(III) and Fe(II) compounds. Coordination of OH^- at neutral pH is fully consistent with the behavior of Fe(III)SOD if we postulate that the metal-associated pK of 9 corresponds to addition of a second OH^- as a sixth ligand rather than to ionization of bound HOH. In the present mechanism, competition between substrate and OH^- for a binding site at Fe(III) would account in part for the pH dependence of K_m.

New evidence supporting the ligation of OH^- to Fe(III)-SOD at neutral pH comes from EXAFS measurements reported in the accompanying paper (Tierney et al., 1995). As noted, assuming OH^- to be the ligand at pH 7.0 requires that the titration of Fe(III) at pH 9 involve addition of a second OH^-. EXAFS spectra at high pH are consistent with formation of the predicted six-coordinate Fe (III) species (Figure 9). The only previous experimental evidence for OH^- as the proton acceptor was a small shift in the position of the solvent ligand in MnSOD on reduction (Ludwig et al., 1991); current analyses of FeSOD indicate a small but statistically insignificant lengthening of the axial Fe–solvent bond, of the order expected for reduction (Table 6).

In order for proton uptake to remain constant near pH 9.0 as observed in measurements of the reduction of Fe(III)-SOD, there must be an ionization in Fe(II)SOD at pH 9 that compensates the ionization at pH 9.0 in Fe(III)SOD. However, the pK of 9.0 in Fe(II)SOD cannot be associated with a metal ligand since the Mössbauer spectra of Fe(II)-SOD at pH 7 and 10 are essentially identical (Niederhoffer et al., 1987; Bull & Fee, 1985). Thus the pKs near pH 9 in the Fe(III) and Fe(II) proteins reflect the ionization of *different* groups, one associated with the metal and the other more distant. We suggest that the Tyr34 OH, which is only 5.4 Å from the metal ion, is the group that titrates at pH 9 in Fe(II)SOD. Its pK would decrease from a value above 10.0 in Fe(III)SOD to approximately 9.0 in Fe(II)SOD. Direct electrostatic interactions between the metal ion and Tyr34 may affect the ionization of the tyrosine. An extensive hydrogen-bonding network centered at Gln69 connects the metal–ligand cluster to the OH of Tyr34 (Figures 5 and 10; Table 6); this set of hydrogen bonds could also provide a structural mechanism for the linkage of the ionization of Tyr34 with events at the metal center. The components of this network are conserved. Tyr34 is invariant in all known Fe and MnSOD structures (Ludwig et al., 1991); residues Gln69 and Gly141 of FeSOD are interchanged for Ala79 and Gln151 in the MnSOD structures but the position of the Gln side chain is similar in Mn- and FeSOD structures (see Figure 10).

Proton Transfers during Turnover. The pH independence of the turnover number and the solvent deuterium isotope effect of approximately 3 (Fee et al., 1986) suggest that proton transfer from H_2O to developing basic centers is partly rate limiting when substrate is saturating. The basic center on the reduced protein that is responsible for proton binding in titration experiments, Fe(II)OH^-, may be a site to which proton transfer is rate limiting during turnover. In the oxidative half-cycle, an additional proton must be taken up to form the product, H_2O_2. In the scheme of Figure 9, species 4 is converted by electron transfer to Fe(III)O_2^{2-}; this basic species is protonated to form Fe(III)-$^-$OOH, which dissociates a hydroperoxyl anion that is subsequently protonated to form peroxide. Specific pathways for proton transfer from water in these steps are not easy to infer from structural data. Moreover the assignment of species involved in proton transfers is notoriously difficult, even with the simplest of reactions.

Although the likely proton donor is HOH (Bull & Fee, 1985), no bound waters other than the metal ligand are visible inside the gate to the metal center that is formed by His30 and Tyr34. On the other hand, a solvent in the substrate funnel is hydrogen-bonded to Tyr34 OH, and several other solvents positioned outside the gate make van der Waals

contacts with His30. We therefore speculate that motions of Tyr34 and His30 may be required for protonation of the coordinated OH^- and of peroxide anion, as well as for coordination of superoxide with the metal ion.

ACKNOWLEDGMENT

Many of the drawings and stereoviews were prepared with the program MAXIM, writtten by M. Rould. We thank Anita Metzger for assistance with the figures and with the preparation of coordinate lists for submission to the Protein Data Bank.

REFERENCES

Bacquet, R. J., McCammon, A. J., & Allison, S. A. (1988) *J. Phys. Chem. 92*, 7134−7141.
Bannister, J. V., Bannister, W. H., & Rotilio, G. (1987) *CRC Crit. Rev. Biochem. 22*, 111−179.
Bertini, I., Luchinat, C., & Monnanni, R. (1985) *J. Am. Chem. Soc. 107*, 2178−2179.
Borgstahl, G. E. O., Parge, H. E., Hickey, M. J., Beyer, W. F., Hallewell, R. A., & Tainer, J. A. (1992) *Cell* 107−118.
Brünger, A. T. (1992) *X-PLOR 3.1*, Yale University, New Haven, CT.
Brünger, A. T., Krukowski, A., & Erickson, J. W. (1990) *Acta Crystallogr. A 46*, 585−593.
Bull, C., & Fee, J. A. (1985) *J. Am. Chem. Soc. 107*, 3295−3304.
Bull, C., Niederhoffer, E. C., Yoshida, T., & Fee, J. A. (1991) *J. Am. Chem. Soc. 113*, 4069−4076.
Callahan, T., Gleason, W. B., & Lybrand, T. P. (1990) *J. Appl. Crystallogr. 23*, 434−436.
Cambillau, C., & Horjales, E. (1987) *J. Mol. Graphics 5*, 174−177.
Carlioz, A., Ludwig, M. L., Stallings, W. C., Fee, J. A., Steinman, H. M., & Touati, D. (1988) *J. Biol. Chem. 263*, 1555−1562.
Chan, V. W. F., Bjerrum, M. J., & Borders, C. L., Jr. (1990) *Arch. Biochem. Biophys. 279*, 195−201.
Davies, G. J., Gamblin, S. J., Littlechild, J. A., & Watson, H. C. (1993) *Proteins: Struct., Funct., Genet. 15*, 283−289.
Dooley, D. M., Jones, T. F., Karas, J. L., McGuirl, M. A., Brown, R. D., III, & Koenig, S. H. (1987) *J. Am. Chem. Soc. 109*, 721−725.
Eriksson, A. E., Baase, W. A., Wozniak, J. A., & Matthews, B. W. (1992) *Nature 355*, 371−373.
Fee, J. A., & McClune, G. J. (1978) *Mechanisms of Oxidizing Enzymes* (Singer, T. P., & Ondarza, R. N., Eds.) pp 273−283, Elsevier/North Holland, Amsterdam.
Fee, J. A., McClune, G. J., Lees, A. C., Zidovetski, R., & Pecht, I. (1981) *Isr. J. Chem. 21*, 54−58.
Fee, J. A., Yoshida, T., Bull, C., O'Neill, P., & Fielden, M. E. (1986) *Superoxide and Superoxide Dismutase in Chemistry, Biology and Medicine* (Rotilio, G., Ed.) pp 205−211, Elsevier, Amsterdam/North Holland.
Fridovich, I. (1974) *Adv. Enzymol. Relat. Areas Mol. Biol. 41*, 35−97.
Getzoff, E. D., Tainer, J. D., Stempien, M. M., Bell, G. I., & Hallewell, R. A. (1989) *Proteins: Struct., Funct., Genet. 5*, 322−336.
Hendrickson, W. A. (1985) *Methods Enzymol. 115*, 252−270.
Kabsch, W., & Sander, C. (1983) *Biopolymers 22*, 2577−2637.
Kraulis, P. J. (1991) *J. Appl. Crystallogr. 24*, 946−950.
Lavelle, F., McAdam, M. E., Fielden, E. M., & Roberts, P. B. (1977) *Biochem. J. 161*, 3−11.
Ludwig, M. L., Pattridge, K. A., & Stallings, W. C. (1986) *Manganese in Metabolism and Enzyme Function* (Wedler, F., & Schramm, V., Eds.) pp 405−430, Academic Press, Inc., New York.
Ludwig, M. L., Metzger, A. L., Pattridge, K. A., & Stallings, W. C. (1991) *J. Mol. Biol. 219*, 335−358.
Matsumoto, T., Terauchi, K., Isobe, T., Matsuoka, K., & Yamakura, F. (1991) *Biochemistry 30*, 3210−3216.
Mendendez-Arias, L., & Argos, P. (1989) *J. Mol. Biol. 206*, 397−406.
Niederhoffer, E. C., Fee, J. A., Papaefthymiou, V., & Munck, E. (1987) *INC Annual Report, Los Alamos National Laboratory*, 79−84.
Ose, D. E., & Fridovich, I. (1979) *Arch. Biochem. Biophys. 194*, 360.
Parker, M. W., & Blake, C. C. (1988) *J. Mol. Biol. 199*, 649−661.
Rardin, R. L., Tolman, W. B., & Lippard, S. J. (1991) *New J. Chem. 15*, 417−430.
Ringe, D., Petsko, G. A., Yamakura, F., Suzuki, K., & Ohmori, D. (1983) *Proc. Natl. Acad. Sci. U.S.A. 80*, 3879−3883.
Schinina, M. E., Maffey, L., Barra, D., Bossa, F., Puget, K., & Michelson, A. M. (1987) *FEBS Lett. 221*, 87−90.
Sines, J., Allison, S., Wierzbicki, A., & McCammon, J. A. (1990) *J. Phys. Chem. 94*, 959−961.
Slykhouse, T. O., & Fee, J. A. (1976) *J. Biol. Chem. 251*, 5472−5477.
Stallings, W. C., Powers, T. B., Pattridge, K. A., Fee, J. A., & Ludwig, M. L. (1983) *Proc. Natl. Acad. Sci. U.S.A. 80*, 3884−3888.
Stallings, W. C., Pattridge, K. A., Strong, R. K., & Ludwig, M. L. (1984) *J. Biol. Chem. 259*, 10695−10699.
Stallings, W. C., Pattridge, K. A., Strong, R. K., & Ludwig, M. L. (1985) *J. Biol. Chem. 260*, 16424−16432.
Stallings, W. C., Metzger, A. L., Pattridge, K. A., Fee, J. A., & Ludwig, M. L. (1991) *Free Rad. Res. Comms. 12−13, part 1*, 259−268.
Stallings, W. C., Bull, C., Fee, J. A., Lah, M. S., & Ludwig, M. L. (1992) *Current Communications in Cell & Molecular Biology 5* (Scandalios, J. G., Ed.) pp 193−212, Cold Spring Harbor Laboratory Press, Plainview, New York.
Stoddard, B. L., Howell, P. L., Ringe, D., & Petsko, G. A. (1990) *Biochemistry 29*, 8885−8893.
Stoddard, B. L., Ringe, D., & Petsko, G. A. (1990) *Protein Eng. 4*, 113−119.
Tainer, J. A., Getzoff, E. D., Beem, K. M., Richardson, J. S., & Richardson, D. C. (1982) *J. Mol. Biol. 160*, 181−217.
Tainer, J. A., Getzoff, E. D., Richardson, J. S., & Richardson, D. C. (1983) *Nature 306*, 284−287.
Tierney, D., Ludwig, M. L., Fee, J. A., & Penner-Hahn, J. E. (1995) *Biochemistry 34*, 1661−1668.
Wagner, U. G., Pattridge, K. A., Ludwig, M. L., Stallings, W. C., Werber, M. M., Oefner, C., Frolow, F., & Sussman, J. L. (1993) *Protein Sci. 2*, 814−825.
Whittaker, J. W., & Whittaker, M. M. (1991) *J. Am. Chem. Soc. 113*, 5528−5540.

BI941514B